ISSN 2029-6991 / eISSN 2029-7009

VILNIUS TECH
Vilnius Gediminas Technical University

GEODESY and CARTOGRAPHY

2026
Volume 52
Issue 1
Pages 21–32
https://doi.org/10.3846/gac.2026.22224

UDC 528.2

ESTIMATING EULER POLE PARAMETERS FOR SUNDALAND BLOCK IN IGB14 USING ROBUST FILTRATION APPROACH

Ahmad Zikri ABD AZIZ[1]✉, Mohamad Asrul MUSTAFAR[1], Mohd Azwan ABBAS[1], Saiful Aman SULAIMAN[2], Muhammad Husaini YA'COB[3]

[1]*Faculty of Built Environment, Universiti Teknologi MARA, Perlis Branch, Arau Campus, 02600 Arau, Perlis, Malaysia*
[2]*Faculty of Built Environment, Universiti Teknologi MARA, Shah Alam, 40450 Shah Alam, Selangor, Malaysia*
[3]*Geodetic Division, Department of Survey and Mapping Malaysia, Level 7&8 Bangunan Ukur, Jalan Sultan Yahya Petra, 50578 Kuala Lumpur, Malaysia*

Article History:
- received 17 September 2024
- accepted 04 March 2026

Abstract. Enhancing the accuracy of the Euler pole parameters for the Sundaland block is essential, given the revised reference frame. The selection of GNSS stations should be obtained before the major event of the 2004 Mw9.2 Sumatra-Andaman earthquake. Initially, 34 GNSS stations in Malaysia, Thailand, Singapore, Indonesia, and Philippines (1999–2004) were adopted under the International Terrestrial Reference Frame 2014 (ITRF2014), specifically IGB14. This study employed precise point positioning (PPP) to obtain accurate coordinates via scientific GipsyX version 1.7. The coordinate time series derived from the X-file mapping approach was utilised to estimate a linear trend motion. The stations' velocities were derived using a 3-dimensional (3D) linear regression approach. To achieve an optimal Euler pole parameter, the outlier filtration processes were employed using statistical tests, limit-based test, and combined statistical and limit-based tests. The combined Baarda and limit-based method was clarified as the robust filtration approach to derive the optimal Euler pole parameters for the Sundaland block at the latitude of 66.77° and longitude of –100.34°, with a rotation rate of 0.302±0.007°/Myr. A further study with densified data covering the maximum Sundaland region is expected to derive the Euler pole parameters more accurately.

Keywords: Euler pole, Sundaland, GNSS, velocities, time series, robust filtration.

✉Corresponding author. E-mail: ***ahmadzikriabdaziz@gmail.com***

1. Introduction

The Sundaland block is encircled by three major tectonic plates; the Philippine Sea Plate, the Australian Plate, and the Indian Plate (Simons et al., 2007). The Eurasian Plate and the Yangtze or South China Block are connected to the north of the Sundaland Block. The Philippine Sea Plate is situated to the east of the Sundaland Plate, whereas the Indo-Australian Plate lies to the west, adjacent to the Sundaland subduction zone and the Sumatran Fault Zone (McCaffrey, 2009). The Sundaland block includes a vast region of contemporary Southeast Asia, consisting of Peninsular Malaysia, Borneo (Sabah, Sarawak, and Brunei), Thailand, Indochina (Vietnam, Cambodia, and Laos), Sumatra, Java, and the shallow maritime areas referred as the Sunda shelf.

GNSS has emerged as a significant space-geodetic instrument for geodynamics research and has been extensively utilised during the past thirty years. The Global Positioning System (GPS) is the foremost GNSS satellite positioning system. GPS campaigns in Eastern Malaysia with intermittent measurements were progressively supplanted by continuous observations. Currently, numerous continuous stations have been created, enhancing the possibility of comprehending the geophysical causes underlying the ongoing tectonic movements (Mustafar et al., 2017). A reliable estimation of the Euler vector can significantly enhance the inference accuracy of long-term fault slip rates (Meade & Hager, 2005), making the enhancement of Euler pole parameter accuracy indispensable. Following the 2004 Mw9.2 Sumatra-Andaman earthquake in the Sunda subduction zone, the assessment of earthquake potential along the Sunda trench has become increasingly critical to avert future disasters. Consequently, enhancing the precision of the Euler pole parameters for the Sundaland plate is essential, given the revised reference frame. The implementation of IGB14, the revised version of ITRF2014, has been emphasised in the domains of

solid earth science, geodesy, and geodynamics research. These disciplines require a globally uniform and enduring terrestrial reference frame to function as a standard reference, ensuring compatibility and coherence among geodetic products. The estimation of the Euler pole parameter for the Sundaland block, as indicated in IGB14, has not yet been performed. Zulkifli et al. (2019) indicated that previous studies conducted in China, Korea, Thailand, and Malaysia revealed that variations in ITRF affected the coordinate systems of these countries. Therefore, it is imperative to enhance the systems to align with the revised global framework (Altamimi et al., 2023). It is essential to obtain the most precise and accurate coordinates by removing the outliers (Mustafar et al., 2017).

The outlier elimination process must employ a robust filtration method instead of the conventional approach that only imposes a set threshold on the data to achieve an optimal Euler pole parameter. This approach will indiscriminately eliminate the station that is above the permissible threshold of residuals. Therefore, it will yield an erroneous distribution of sites in determining the Euler pole parameter. Thus, more research is necessary to address the concerns related to the current filtration process. A robust approach should be stressed to regulate the dispersion of the CORS to systematically calculate the Euler pole parameters of the Sundaland plate. Furthermore, a robust technique can secure the stations by the assessment of data quality to maintain the number of verified CORS, which ultimately regulates the distribution of stations. It is essential to prioritise the selection of the dataset timeframe when estimating the Euler pole parameter. The data used must be free from any effects of seismic activity to ensure the accuracy of the predicted Euler pole as well as the selection of CORS for assessing the motion of the Sundaland plate should be obtained prior to the major event of the 2004 Mw9.2 Sumatra-Andaman earthquake (Mustafar et al., 2017). This study presents the Euler pole parameters of the Sundaland plate under the IGB14 and highlights various filtration methods, including the Baarda test, Tau test, limit-based test, and combinations of the Baarda test and limit-based methods, as well as the Tau test and limit-based test, to enhance the reliability of the pole parameters. Moreover, we conducted additional validation of the prior models and provided insights into the movement of the Sundaland plate, constrained by GNSS locations, before the 2004 Mw9.2 Sumatra-Andaman earthquake.

2. GNSS data

The data in this study were mostly gathered through recent collaborations between European (Netherlands and France) and Asian (Malaysia, Thailand, and Indonesia) institutions and government organisations (for example, in the EU-ASEANSEAMERGES and GEO2TECDI programs). Continuous GNSS stations were utilised to compute the Sundaland plate's absolute pre-seismic motion before the massive impact of the 2004 Sumatra-Andaman earthquake (Mw 9.2). GNSS data from 34 local continuous stations in Malaysia, Thailand, Singapore, Indonesia, and the Philippines from 1999 to Boxing Day 2004 (Figure 1). These

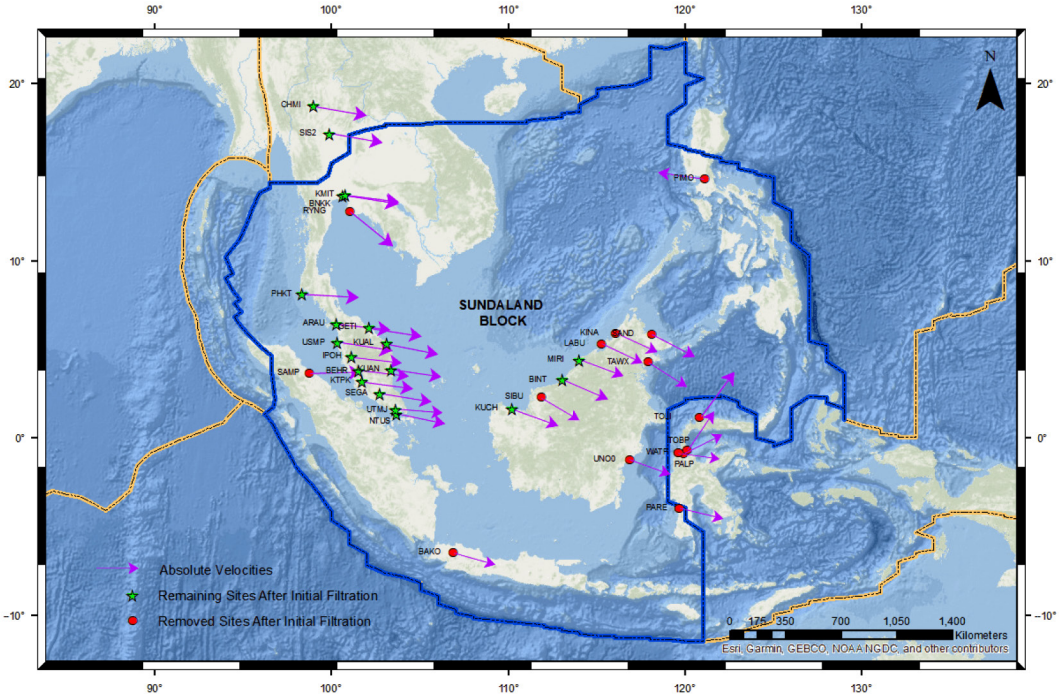

Note: Purple arrows indicate absolute velocities derived from coordinate time series in IGB14; Green stars indicate remaining stations after the initial filtration process; Red circles denote excluded stations after the initial filtration process; Blue lines denote boundaries of Sundaland block; Orange lines represent boundaries of the plates surrounding Sundaland block.

Figure 1. Distribution of GNSS stations for this study in Southeast Asia (1999–2004) prior to the massive impact of the 2004 Sumatra-Andaman earthquake (Mw 9.2)

three nations, in conjunction with Laos, Cambodia, and Vietnam, constitute the principal component of the Sundaland block.

In Malaysia, 18 continuous stations encompass Peninsular Malaysia (ten stations) and Borneo (eight stations). Additional stations are situated in Thailand (six stations), Indonesia (eight stations), Singapore (one station), and the Philippines (one station). Final GNSS solutions comprise three-dimensional (3D) station coordinates. The coordinates are time-dependent owing to tectonic plate movement and any displacements caused by earthquakes, both co-seismic and post-seismic. Representing these coordinates in the IGB14 (the updated version of ITRF2014) will yield valuable solutions inside a unified global reference frame. The initial phase of outlier elimination was analysed via the output of absolute velocities (Table 1) by delineating the magnitude and direction of each site. In this step, 15 sites were excluded based on the rejection criterion, while 19 remaining sites were employed to determine the optimal Euler pole parameters of the Sundaland block using a robust filtration method.

Table 1. GNSS stations used in this study for the determination of Sundaland pole parameters

Sites	Latitude (°)	Longitude (°)	Vn (mm/yr)	Ve (mm/yr)	Sigma Vn (mm/yr)	Sigma Ve (mm/yr)	Data Timespan
ARAU	6.450	100.280	–3.37	33.39	0.32	0.34	1999.00–2004.98
BAKO	–6.491	106.849	–6.54	23.43	0.18	0.22	1999.00–2005.00
BEHR	3.765	101.517	–3.66	31.39	0.44	0.52	2002.61–2004.98
BINT	3.262	113.067	–11.84	27.50	0.21	0.25	1999.09–2005.00
BNKK	13.668	100.607	–5.21	33.71	0.30	0.34	2001.60–2004.98
CHMI	18.771	98.973	–5.51	32.28	0.28	0.32	2001.57–2004.98
GETI	6.226	102.105	–4.91	32.35	0.17	0.20	1999.00–2004.83
IPOH	4.588	101.126	–3.51	31.48	0.29	0.35	1999.25–2004.95
KINA	5.905	116.039	–11.61	25.40	0.19	0.22	1999.04–2004.99
KMIT	13.731	100.778	–4.17	32.63	0.33	0.39	2002.33–2004.98
KTPK	3.171	101.718	–4.21	31.69	0.16	0.19	1999.23–2004.97
KUAL	5.319	103.139	–6.32	32.01	0.19	0.22	1999.00–2004.98
KUAN	3.834	103.350	–4.52	31.32	0.18	0.21	1999.17–2004.98
KUCH	1.632	110.195	–10.04	27.96	0.41	0.42	1999.00–2003.49
LABU	5.283	115.245	–11.91	24.97	0.18	0.21	1999.26–2005.00
MIRI	4.372	114.002	–9.94	26.71	0.16	0.19	1999.21–2004.98
NTUS	1.346	103.680	–6.35	30.53	0.16	0.18	1999.02–2004.98
PALP	–0.916	119.906	9.91	19.53	0.32	0.36	2002.43–2005.00
PARE	–3.978	119.650	–5.95	25.01	0.20	0.23	1999.50–2005.00
PHKT	8.105	98.308	–1.88	34.03	0.30	0.36	2001.58–2004.98
PIMO	14.636	121.078	4.11	–28.69	0.30	0.33	1999.30–2005.00
RYNG	12.764	101.033	–22.03	27.35	8.31	9.92	2004.18–2004.95
SAMP	3.622	98.715	0.81	32.50	0.19	0.23	1999.00–2004.98
SAND	5.842	118.121	–14.12	27.02	0.20	0.23	1999.39–2005.00
SEGA	2.486	102.732	–5.11	31.58	0.23	0.27	2001.11–2004.94
SIBU	2.270	111.843	–12.59	21.40	0.32	0.37	2001.13–2004.92
SIS2	17.157	99.867	–5.77	32.88	0.30	0.34	2000.69–2004.98
TAWX	4.263	117.882	–14.59	22.91	0.24	0.27	1999.39–2005.00
TOBP	–0.709	120.095	23.67	16.01	0.24	0.26	2001.02–2005.00
TOLI	1.121	120.794	29.79	21.93	0.43	0.47	2001.09–2004.73
UNO0	–1.269	116.826	–8.68	23.89	0.87	0.97	2003.45–2004.98
USMP	5.358	100.304	–5.35	34.93	0.21	0.25	1999.94–2004.98
UTMJ	1.566	103.640	–2.31	29.19	0.19	0.22	1999.11–2004.98
WATP	–0.874	119.587	–2.69	20.36	0.21	0.25	2001.02–2005.00

3. GNSS data processing

Dual-frequency GNSS data were analysed using the scientific GipsyX software version 1.7 (Jet Propulsion Laboratory 2013). This study employed precise point positioning (PPP) to obtain accurate coordinate data (Zumberge et al., 1997). The Jet Propulsion Laboratory (JPL) provided precise satellite ephemeris and Earth rotation parameters, allowing for the consistent derivation of highly accurate daily absolute GNSS positioning results (Mustafar et al., 2017).

3.1. Daily solutions

The GNSS data were reduced to 5-minute intervals. The data were processed using zero-differencing into daily coordinates, utilising the ionospheric-free combination of the observables. An elevation mask angle of 7 degrees (°) was employed. Absolute IGS antenna phase center corrections were implemented to account for the systematic inaccuracies associated with varying elevation angles and azimuths of the monitored satellites. The IGB14 absolute antenna phase centre table was obtained in conjunction with the weekly JPL orbits and clock products. Elevation mask angles may be less than 10° when employing absolute phase center variation tables (Schmid et al., 2005). The tropospheric mapping function employed is the Vienna Mapping Functions (VMF1), derived from numerical data reflecting actual meteorological conditions. The VMF1 mapping coefficient grid database was obtained from the Global Geodetic Observing System website, operated by the Vienna University of Technology (Boehm et al., 2006). Lyard et al. (2006) integrated satellite altimetry (TOPEX/POSEIDON) data into their hydrodynamic tide model to generate FES2004. This model is one of the standard global ocean tide models in addition to GOT4.7 (Mustafar et al., 2017). Consequently, FES2004 was utilised in the processing, and the ocean loading parameters were obtained from the Onsala Space Observatory website (Bos & Scherneck, 2014). To improve the coordinate solutions in the east-west direction in this area, ambiguity resolution has been implemented utilising the Ambizap algorithm (Blewitt, 2008). Ambizap offers distinctive ambiguity-resolved single-network solutions. Furthermore, Ambizap offers a direct and rapid method for incorporating additional consistent station data into an existing and processed network, attributable to the nature of PPP solutions, which are uncorrelated with other stations due to their zero-differenced processing characteristics (Mustafar et al., 2017).

3.2. GNSS coordinate time series

The coordinate time series derived from the X-file mapping approach for the 1999–2004 data period was utilised to estimate a linear trend motion for each station. The velocities of the stations were derived using a 3-dimensional (3D) linear regression approach applied to the coordinate time series, which estimates position lifts. In the vertical direction, following Blewitt and Lavallée (2002), seasonal variation was represented as $A*\sin(\alpha) + B*\cos(\alpha)$, where α equals 360°/365.25 days multiplied by the number of days since the initial data epoch. Parameters A and B were determined in conjunction with the linear regression algorithm. The upper limit of linear misfits at a 99% confidence level was established at ±7.5 mm, ±10.1 mm, and ±18.8 mm for the north, east, and vertical components, respectively, to detect any outliers in the velocity calculation (as shown in Figure 2).

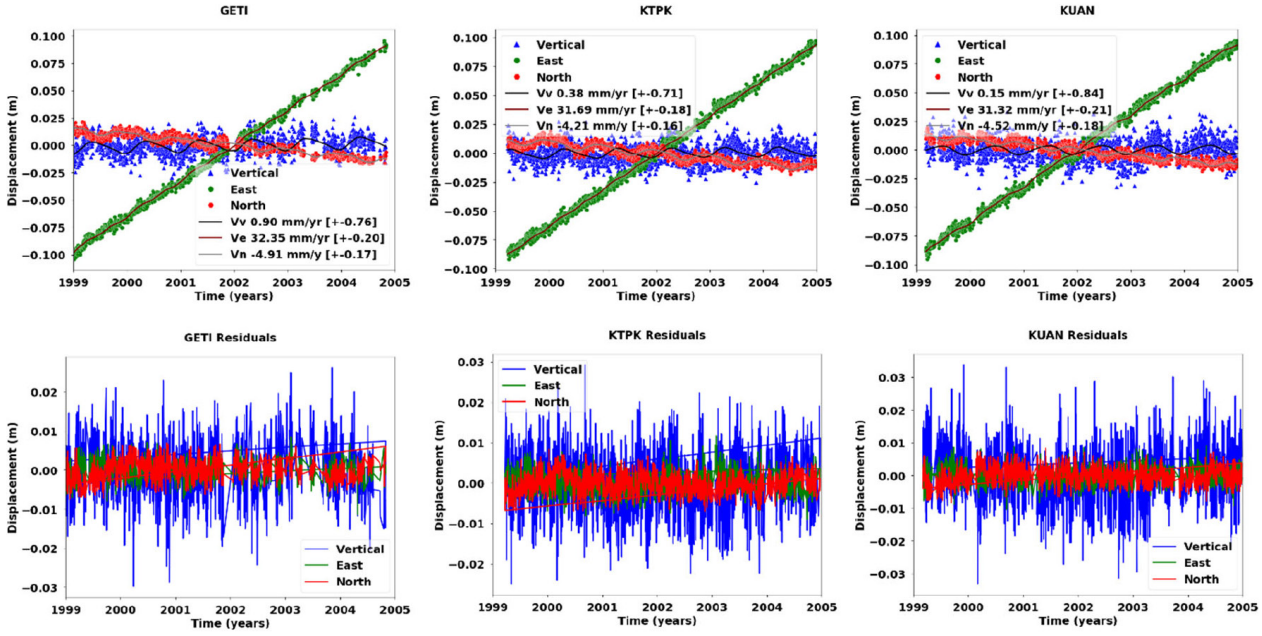

Figure 2. Examples of coordinate time series (CTS) and residuals graphs for station GETI, KTPK, and KUAN using precise point positioning (PPP) in GipsyX1.7 software

The criteria for outlier detection concerning absolute velocities are founded on the error propagation of daily coordinate repeatabilities and the misfits of IGS station positions in IGB14. They incorporate additional tolerances of 2 mm and 4 mm for noted seasonal fluctuations in the horizontal and predominantly affected vertical coordinate time series, respectively. The standard errors (99% confidence level) for each linear estimation are derived via a Weighted Root Mean Square (WRMS) approach defined as (2*WRMS)/T, where T represents the whole observation time in years (Simons et al., 2007). This strategy has demonstrated itself as a straightforward and secure approach to ensuring that velocity errors are realistic, as formal errors derived from least-squares adjustment methods are generally overly optimistic, and it was tested by Simons et al. (2007) against methods based on empirical noise models.

4. Sundaland block motion

The Sundaland platelet's boundaries were established using strain-rate tensor analysis, except for the northwest, where the geological boundary between Sundaland and the South China blocks was employed (Simons et al., 2007). The motion of a plate(let) can be characterised by a vector and a pole of rotation, as per Euler's rotation theorem (Mustafar et al., 2017). The block motion can be approximated using the velocity vectors of GNSS stations on Sundaland. The study utilised six years of coordinated time series to determine the velocity of stations from 1999 to 2004 in IGB14. Data from 26 December 2004 onwards were excluded to prevent the incorporation of station positions influenced by co- and post-seismic movements resulting from the Sumatra-Andaman earthquake event (Vigny et al., 2005). The pre-seismic velocities were utilised to ascertain an IGB14-compatible rotation rate and pole for Sundaland.

4.1. Previous estimates for Sundaland block motion

Numerous estimations of the Sundaland block exist, with the majority published after 2002, with the release of ITRF2000 (Table 2). All these estimations utilise GNSS data from Sundaland during the pre-seismic period (1994–2004). The output before 2002 was inaccurate owing to the poorly defined ITRF1994 and ITRF1997 reference frames.

Kreemer et al. (2003) formulated an innovative no-net-rotation (NNR) model by integrating geodetic site velocities with geological strain rates. The NNR-GSRM1 reference frame indicates alignment with ITRF2000 in this area (Simons et al., 2007). The solutions provided by Bock et al. (2003), Simons et al. (2007), DeMets et al. (2010), and Argus et al. (2011) yield comparable results while employing distinct station selections and reference frames. The estimation by Prawirodirdjo and Bock (2004) presents the lowest pole latitude and the highest rotation rate; nevertheless, it relied solely on two stations, BAKO (Java) and NTUS (Singapore), leading to a less precise outcome. Station BAKO demonstrates a more unstable coordinate time series and is situated in proximity to the Australian-Sundaland plate boundary.

Simons et al. (2007) delineated the motion and boundaries of the Sundaland block. They utilised 28 stations to assess the motion of the Sundaland block in ITRF2000, representing the biggest number of stations at present. Their integration of campaigns and continuous stations yielded an excellent result. Their motion was revised with the identical GNSS dataset and locations on Sundaland in ITRF2005, demonstrating the varying velocity estimates derived from ITRF2005 compared to ITRF2000. Subsequently, DeMets et al. (2010) employed 18 station velocities from Simons et al. (2007) in their estimation of Sundaland. This is a reduction of 10 stations compared to the study by Simons et al., attributable to the proximity of these sites to the Sumatra Trench, with one situated on the island

Table 2. Absolute Euler pole parameters for the Sundaland block

Source	Ref. Frame	Sites	Euler pole parameters (Sundaland)		
			Latitude (°)	Longitude (°)	Rate (°/Myr)
(Kreemer et al., 2003)	NNR-GSRM1	9	47.3	–90.13	0.392±0.008
(Bock et al., 2003)	ITRF2000	16	49.8	–95.9	0.320±0.010
(Prawirodirdjo & Bock, 2004)	ITRF2000	2	32.6	–86.8	0.462±0.064
(Kreemer et al., 2006)	ITRF2000	21	43.6	–89.6	0.366±0.013
	NNR-GSRM2	–	44.3	–88.8	0.387±0.012
(Simons et al., 2007)	ITRF2000	28	49.0	–94.2	0.336±0.007
Simons (pers. comm. 2012)	ITRF2005	28	52.1	–90.9	0.322±0.007
(DeMets et al., 2010)	ITRF2000	18	48.5	–93.9	0.326
(Argus et al., 2011)	NNR-MORVEL56	–	50.1	–95.1	0.337±0.020
(Altamimi et al., 2012)	ITRF2008	2	44.2	87.3	0.388±0.308
(Mustafar et al., 2017)	IGS08 (ITRF2008)	14	48.05	–88.51	0.341±0.015
(Yong et al., 2017)	ITRF2014	10	44.16	–87.22	0.349±0.038
This study (Baarda+Limit)	IGB14 (ITRF2014)	13	66.77	–100.34	0.302±0.007

of Java. Nonetheless, their estimations for the Sundaland pole location and rotation rate remain nearly unchanged. Subsequently, Argus et al. (2011) employed the results of the MORVEL model from DeMets et al. (2010) to establish their NNR-MORVEL56 model. The NNR-MORVEL56 is regarded as the premier plate model currently, including 99.8% of the Earth's surface, with 25 major and 31 minor plates (Bird, 2003; DeMets et al., 2010).

Altamimi et al. (2012) identified the latest solution in their study on plate motions in ITRF2008 to assess the appropriateness of NNR-MORVEL56 for future ITRF solution releases. Their motion estimates for Sundaland relied solely on the two stations in Peninsular Malaysia (GETI and NTUS) incorporated in the ITRF2008. This solution is not limited to the northern and eastern regions of Sundaland. Before the 2004 Mw 9.2 Sumatra-Andaman earthquake, the GETI station exhibited an accelerated steady-state velocity resulting from inter-seismic loading of the immobilised subduction interface off the coast of Sumatra, which facilitates the convergence of the Indian and Australian plates with Sundaland (Simons et al., 2007). The co-seismic displacement at GETI resulting from the Mw9.2 earthquake was considerably greater than that recorded at NTUS (Vigny et al., 2005). Utilising solely NTUS and GETI, the findings of Altamimi et al. (2012) could be replicated with an accuracy of 0.3° in latitude/longitude and 0.01/Myr in rotation rate.

Their comprehensive findings demonstrated that ITRF2008 plate motion estimates exhibit superior concordance with NNR-MORVEL56 compared to NNR-NUVEL1A. NNR-NUVEL1A is a recognised no-net rotation frame comprising a collection of geological angular velocities from 14 tectonic plates (Argus & Gordon, 1991). It is less relevant for our research as it lacks a definition for Sundaland, which is seen as the remaining part of Eurasia. However, the considerable discrepancy in rotation rates between NNR-MORVEL56 and ITRF2008 shows that ITRF2008's alignment accuracy with NNR-MORVEL56 is less than 2 mm/year (Altamimi et al., 2012). Ultimately, ITRF2000 velocities exhibit incompatibility with both ITRF2005 and ITRF2008, as the velocities in the latitude component (particularly in Southeast Asia) have been seen to vary by several millimeters each year (Satirapod et al., 2011) hence influencing the predictions of the Euler pole and rotation rate.

We want to highlight that any efforts to reevaluate the Sundaland motion utilising or incorporating GNSS data subsequent to 26 December 2004 from Cambodia, Laos, Thailand, Vietnam, Peninsular Malaysia, western Indonesia, and West Borneo must consider (through geophysical modelling) the post-seismic motions resulting from the Mw 9.2 Sumatra-Andaman earthquake. Stations in Peninsular Malaysia and Singapore continue to demonstrate considerable horizontal displacement rate offsets between 10 and 25 mm/year in the WSW direction when comparing their inter-seismic velocity estimates from 1999 to 2004 (Mustafar et al., 2017). Despite a gradual decrease in intensity, post-seismic movement may persist in this region for decades. Mustafar et al. (2017) and Yong et al. (2017) have recently computed the Euler pole parameters for Sundaland utilising data from 1999 to 2004. Nonetheless, the reliability of these methods is dubious owing to the presence of unstable stations. The outlier filtration strategies employed by Mustafar et al. (2017) and Yong et al. (2017), which utilised a limit-based approach with residual thresholds of 3 mm per year and 10 mm per year, respectively, were insufficient to ensure the quality of the stations. The focus should be on the integration of limit-based and statistical analysis to enhance the outlier removal procedure.

4.2. Euler pole parameter estimation for Sundaland block

A revised absolute rotation pole and rate for the Sundaland plate must be calculated, since the solution in IGB14 (ITRF2014) has not yet been performed. The resultant rotation solution relies on the chosen stations presumed to be part of undeformed Sundaland. Consequently, the selection of these stations necessitates the delineation of the Sundaland block boundaries. Nonetheless, not all the stations in Sundaland are situated within the central core of this plate; some are also found on its extensive limits, which are influenced by nearby plates undergoing deformation. Therefore, stations situated near active faults, plate boundary zones, and influenced by local ground motions must be eliminated from the computations as a preliminary filtration (Figure 1). 15 of the 34 stations were eliminated during the preliminary filtration. The remaining 19 stations were subjected to subsequent filtration methods, including limit-based test, statistical tests, and a combination of limit-based and statistical tests, to determine the most robust filtration approach for quantifying optimal Euler pole parameters for the Sundaland block. A threshold limit of 3 mm/year for residual velocities was established as a rejection criterion for a limit-based test, given that the majority of the estimated horizontal velocities in Southeast Asia (1999–2004) possess a 99% confidence level of approximately 1.0 mm/year, with potential intra-plate deformation of ±1 mm/year (Mustafar et al., 2017; Simons et al., 2007). The Baarda and Tau tests were employed to eliminate outliers over the rejection threshold (Ghilani & Wolf, 2006; Goudarzi et al., 2014). Furthermore, the integration of limit-based and statistical testing underscored both previously described rejection phases. Multiple iterations were conducted across all methods to identify and eliminate stations impacted by local motions or displaying erroneous velocity estimates due to other inaccuracies. The iterative process persisted until all remaining stations met the rejection requirement.

At last, 15 stations were included in the final estimation of the revised Euler pole parameters for the Sundaland block, utilising both limit-based and statistical tests (Baarda and Tau). Simultaneously, 13 and 11 stations continued to employ the combined Baarda and limit-based

tests, along with the Tau and limit-based tests, respectively (Table 3). The final solution in IGB14 (an updated version of ITRF2014) presents the Euler pole parameters of Sundaland utilising the Baarda and Tau method, situated at a latitude of 61.60° and longitude of –95.62°, with a rotation rate of 0.312±0.010°/Myr. In contrast, the limit-based method identifies the location at a latitude of 65.79° and longitude of -99.00°, with a rotation rate of 0.306±0.009°/Myr. The Euler pole for Sundaland, determined using a combined Baarda and limit-based method, is situated at a latitude of 66.77° and a longitude of –100.34°, with a rotation rate of 0.302±0.007°/Myr. In contrast, a combined Tau and limit-based method identified the Sundaland pole at a latitude of 67.47° and a longitude of –101.73°, with a rotation rate of 0.300±0.006°/Myr. Additionally, the Euler pole for Sundaland was reestimated in IGB14 using the site selection from prior studies (Mustafar et al., 2017; Yong et al., 2017) to facilitate a comparison of the solutions with our findings, as the data timeframe (1999–2004) aligned with our study and the availability of their selected sites. The Euler pole parameters for Sundaland were determined using 14 stations from Mustafar and 10 stations from Yong, yielding a latitude of 47.91° and longitude of –88.49° with a rotation rate of 0.354±0.024°/Myr, and a latitude of 39.24° and longitude of –85.28° with a rotation rate of 0.392±0.042°/Myr.

Table 3. Absolute Euler pole parameters for the Sundaland block from six solutions of this study

Source	Ref. Frame	Sites	Euler pole parameters (Sundaland)		
			Latitude (°)	Longitude (°)	Rate (°/Myr)
Baarda & Tau	IGB14	15	61.60	–95.62	0.312±0.010
Limit	IGB14	15	65.79	–99.00	0.306±0.009
Baarda + Limit	IGB14	13	66.77	–100.34	0.302±0.007
Tau + Limit	IGB14	11	67.47	–101.73	0.300±0.006
Mustafar (Re-estimated)	IGB14	14	47.91	–88.49	0.354±0.024
Yong (Re-estimated)	IGB14	10	39.24	–85.28	0.392±0.042

The residuals in the Northing and Easting components of all the selected stations, which were analysed using a combination of Baarda and limit-based methods, as well as Tau and limit-based methods, were less than 2 mm/year (Table 4). The residuals of two stations exceed 2 mm/year for single statistical (KUCH and PHKT) and limit-based (PHKT and USMP), while the residuals of the remaining stations are less than 2 mm/year. In the solution from Mustafar, one station (SIS2) has residuals exceeding 2 mm/year, and two stations (BINT and UTMJ) have residuals exceeding 3 mm/year. Conversely, the solution

Table 4. Velocity residuals of each station used from six solutions in this study

Sites	Baarda & Tau (mm/yr)		Limit (mm/yr)		Baarda + Limit (mm/yr)		Tau + Limit (mm/yr)		Mustafar Re-Estimated (mm/yr)		Yong Re-Estimated (mm/yr)	
	Resid North	Resid East	Resid North	Resid East	Resid North	Resid East	Resid North	Resid East	Resid North	Resid East	Resid North	Resid East
ARAU	1.15	1.31	1.24	1.04	1.30	1.33	–	–	–	–	–	–
BAKO	–	–	–	–	–	–	–	–	–	–	0.56	–0.25
BEHR	1.21	–0.08	1.24	–0.47	1.28	–0.22	1.40	–0.18	0.93	0.54	–	–
BINT	–	–	–	–	–	–	–	–	–2.15	–3.05	–1.21	–1.87
BNKK	–0.59	0.34	–0.52	0.42	–0.47	0.80	–0.34	0.93	–1.04	–0.82	–	–
CHMI	–1.35	–1.73	–1.20	–1.41	–1.12	–0.97	–0.98	–0.80	–	–	–	–
GETI	0.11	0.33	0.12	0.06	0.15	0.34	0.26	0.40	–0.06	0.51	–0.57	1.28
IPOH	1.25	–0.18	1.30	–0.54	1.34	–0.27	–	–	0.90	0.29	–	–
KMIT	0.49	–0.76	0.56	–0.67	0.61	–0.29	0.74	–0.16	0.08	–1.93	–	–
KTPK	0.71	0.37	0.73	–0.05	0.76	0.19	0.88	0.23	0.46	1.09	–	–
KUAL	–1.01	0.19	–1.06	–0.13	–1.04	0.15	–0.94	0.20	–1.01	0.53	–1.37	1.43
KUAN	0.85	–0.15	0.79	–0.55	0.81	–0.29	0.91	–0.25	0.89	0.45	0.55	1.55
KUCH	–2.85	–2.95	–	–	–	–	–	–	–1.59	–1.95	–1.02	–0.55
MIRI	–	–	–	–	–	–	–	–	–	–	1.22	–3.24
NTUS	–0.89	–0.32	–0.97	–0.83	–0.96	–0.61	–0.86	–0.60	–0.79	0.72	–1.09	2.15
PHKT	2.09	1.58	2.27	1.39	–	–	–	–	–	–	–	–
SEGA	0.09	0.43	0.06	–0.03	0.09	0.21	0.20	0.24	0.03	1.27	–	–
SIBU	–	–	–	–	–	–	–	–	–	–	–2.64	–7.46
SIS2	–1.36	–0.95	–1.26	–0.70	–1.20	–0.28	–1.06	–0.12	–1.94	–2.73	–	–
USMP	–	–	–0.73	2.77	–	–	–	–	–	–	–	–
UTMJ	–	–	–	–	–	–	–	–	3.23	–0.71	2.93	0.69

from Yong has one station (NTUS) with residuals exceeding 2 mm/year, one station (MIRI) with residuals exceeding 3 mm/year, and one station (SIBU) with residuals exceeding 7 mm/year.

The stations in Thailand, Singapore, and Borneo display a residual component directed southward. Concurrently, the majority of stations in Peninsular Malaysia exhibit analogous deformation characteristics towards the north at a rate of 1–2 mm/year (Figure 3), attributable to the influence of the Indian/Australian plate subduction interface (strain accumulation preceding the 2004 Sumatra-Andaman earthquake) beneath Sumatra.

The analogous directions of the residuals in these regions demonstrate that intra-plate deformation of Sundaland is taking place significantly distant from its plate boundaries (e.g., because of elastic loading) up to 750 km away from its boundary with the subducting Indian and Australian plates to the west (Mustafar et al., 2017; Simons et al., 2007).

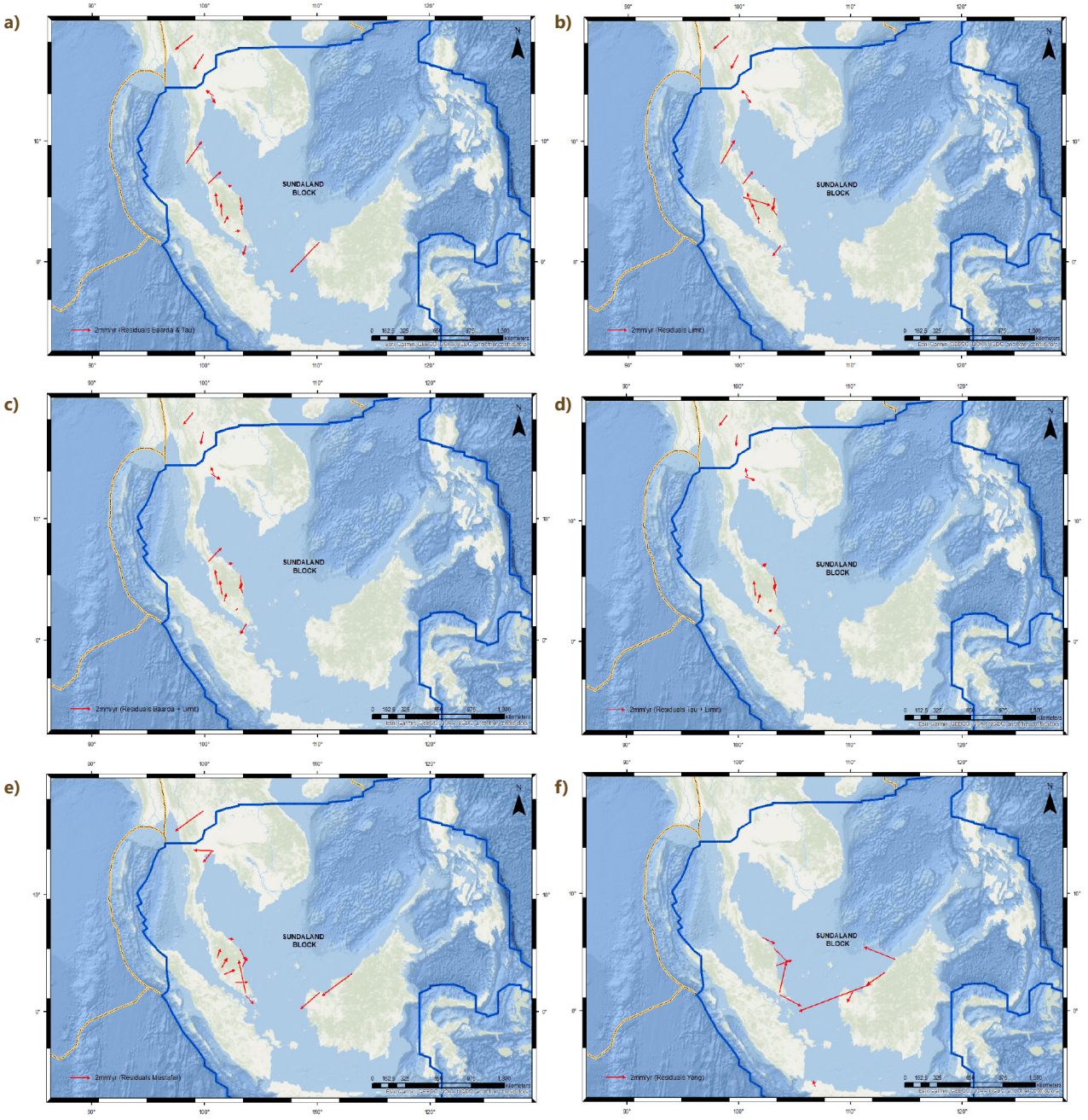

Note: Red arrows indicate the magnitude and direction of the stations' residuals: a) velocity residuals using Baarda and Tau filtration (15 stations used); b) velocity residuals using limit-based filtration (15 stations used); c) velocity residuals using combined Baarda and limit-based filtration (13 stations used); d) velocity residuals using combined Tau and limit-based filtration (11 stations used); e) velocity residuals using selected stations that were defined by Mustafar et al. (2017) (14 stations used); f) velocity residuals using selected stations that were defined by Yong et al. (2017) (10 stations used).

Figure 3. Map of velocity residuals for each station

5. Discussion

Several analysis have been performed to examine the reliability of the four proposed methods in this study, which is to determine the most robust method for the optimal Euler pole parameter estimation. The Euler pole parameters from the selected sites by the previous studies (Mustafar et al., 2017; Yong et al., 2017) in IGB14 were used to compare their solutions with our study. First and foremost, the Root Mean Squared Error (RMSE) of the velocity residuals was computed to analyse the quality of the solutions in terms of average from the total error distribution. Based on Figure 4, we can observe that the four proposed methods (Baarda and Tau, limit-based, combined Baarda and limit-based, combined Tau and limit-based) in this study have significantly lower residuals RMSE compared to the solutions from the previous studies. It indicates that the outlier filtration approaches that were defined in this study should be emphasized in estimating the Euler pole parameters of the tectonic plates, specifically the Sundaland block. Among the results from the four proposed methods, the combined statistical and limit-based methods produced a lower RMSE value rather than the solutions from a single statistical or limit-based method. Besides, both combined methods provide almost equivalent results of residuals RMSE for all three components (magnitude, northing, and easting).

In addition, Figure 5 depicts the percentage of the distribution for the total horizontal magnitude of the residuals by each solution that does not exceed 2 mm/year. The results from the selected sites by Mustafar et al. (2017) and Yong et al. (2017) indicate that the residual magnitude distribution not exceeding 2 mm/year was below 80% whereas more than 80% was acquired by single statistical or limit-based method. Meanwhile, the combined methods of statistical and limit-based achieved 100% of the stations that have residuals of the magnitude below 2 mm/year.

For further analysis of the results, the histogram in Figure 6 illustrates the results of the combination of statistical and limit-based methods (combined Baarda and limit-based, and combined Tau and limit-based) in this study show the residuals of all components (magnitude, northing, and easting) with a more-centered distribution compared to other four solutions. The limit-based method is capable of securing the distribution of the stations with low residuals whereas the statistical tests have the potential to sustain the quality of data by eliminating the outliers based on the standard deviation. Hereby, the combination of these methods was highly recommended to enhance the robustness of the outlier filtration strategy. Since the results of both combined methods were almost identical, we concluded the combined Baarda and limit-based method was the superior method as the robust filtration approach in quantifying the optimal Euler pole parameters for Sundaland block rather than the combined Tau and limit-based method due to the number of remaining stations after the last iteration of the outlier filtration process which is 13 and 11 stations (Table 3), respectively.

Ten (10) random sites were established that covered the region within the Sundaland block to observe the results of the estimated velocities from Sundaland pole rotation of each solution (Figure 7). The west and north Sundaland produced almost similar directions and magnitudes of the velocities. Meanwhile, the difference in the

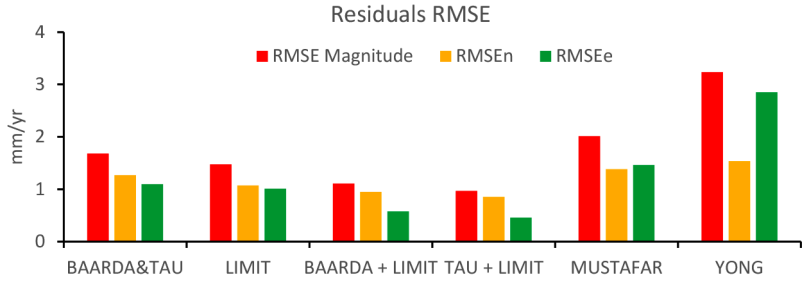

Note: Red bars indicate residuals RMSE for magnitude component; Orange bars denote residuals RMSE for northing component; Green bars represent residuals RMSE for easting component.

Figure 4. Graph of Root Mean Squared Error (RMSE) of residuals for each solution

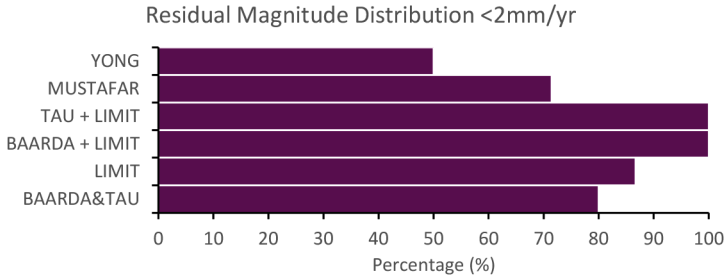

Figure 5. Graph of the distribution percentage for the total horizontal magnitude of the residuals by each solution that does not exceed 2 mm/year

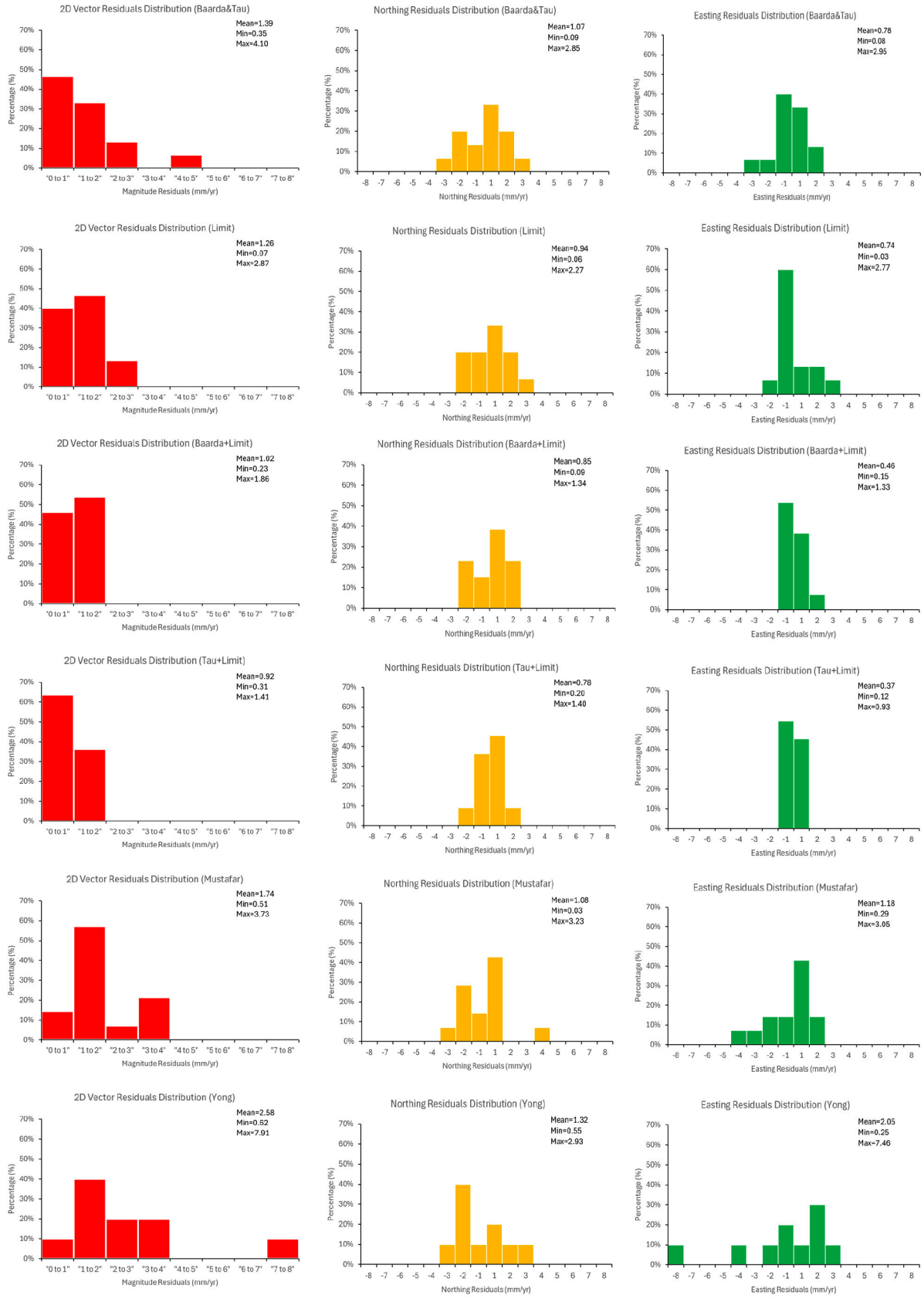

Note: The first row represents the solution from Baarda and Tau tests, the second row represents the solution from limit-based tests, the third row represents the solution from combined Baarda and limit-based tests, the fourth row represents the solution from combined Tau and limit-based tests, the fifth row represents the solution from the selected sites by Mustafar et al. (2017), and the sixth row represents the solution from the selected sites by Yong et al. (2017). Mean indicates the mean value of the distribution; Min denotes the minimum value of the distribution; Max represents the maximum value of the distribution; Red bars indicate the residuals distribution of the 2-dimensional vector; Orange bars denote the residuals distribution of the northing component; Green bars represent the residuals distribution of the easting component.

Figure 6. Velocity residuals histogram using Sundaland pole rotation from six solutions. The bin width is 1 mm/year for the northing and easting residuals components

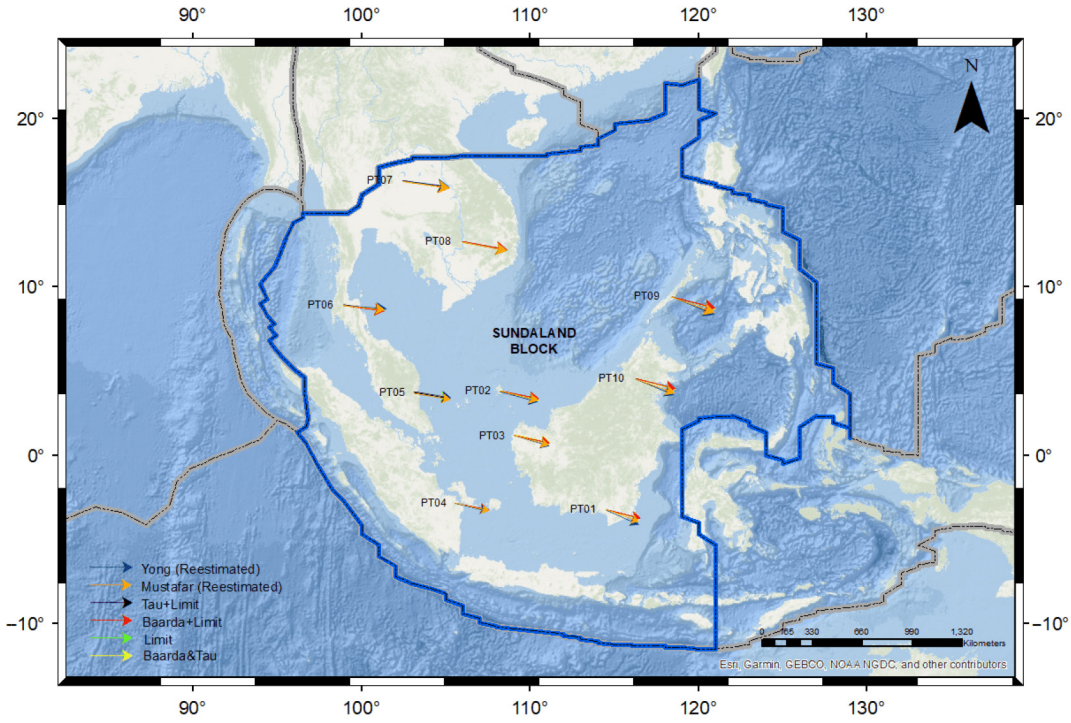

Note: Yellow arrows indicate estimated velocities with respect to Sundaland using Euler pole from Baarda and Tau tests; Green arrows denote estimated velocities with respect to Sundaland using Euler pole from the limit-based test; Red arrows represent estimated velocities with respect to Sundaland using Euler pole from combined Baarda and limit-based tests; Black arrows indicate estimated velocities with respect to Sundaland using Euler pole from combined Tau and limit-based tests; Orange arrows denote estimated velocities with respect to Sundaland using the re-estimated Euler pole from selected sites by Mustafar et al. (2017); Blue arrows represent estimated velocities with respect to Sundaland using the re-estimated Euler pole from selected sites by Yong et al. (2017).

Figure 7. Site validation from 10 selected sites of each region within Sundaland block using six solutions of Sundaland pole rotation

velocities' direction appeared at the east and south Sundaland between the solution from the re-estimation of previous studies (Mustafar et al., 2017; Yong et al., 2017) and the solutions from this study. It indicates that the site selection in estimating the Sundaland pole rotation is very crucial to ensure that all selected sites are free from outliers or local motion.

6. Conclusions

We first processed the GNSS data from 34 sites within Sundaland using the data timeframe from 1999 to 2004, which is prior to the massive impact of 2004 Mw9.2 Sumatra-Andaman earthquake to evaluate the Euler pole parameters of Sundaland plate in IGB14 (updated version of ITRF2014). The stations situated near active faults, plate boundary zones, and influenced by local ground motions were eliminated from the computations as a preliminary filtration. To improve the reliability of parameter estimation, we proposed four outlier filtration approaches to identify the robustness of these methods. In addition, the re-estimation of Sundaland pole rotation was conducted using the selected sites by previous studies in IGB14 to compare their solutions with our study. Based on the result and analysis, both combined statistical and limit-based produced good results in terms of RMSE and mean distribution of the velocity residuals. However, the combined Baarda and limit-based method secured more stations with well-distribution. Therefore, this method was clarified as the robust filtration approach to derive the optimal Euler pole parameters for the Sundaland block at the latitude of 66.77° and longitude of –100.34°, with a rotation rate of 0.302±0.007°/Myr. A further study with denser data that covers the maximum region of the Sundaland block is expected to derive the Euler pole parameters with greater accuracy.

References

Altamimi, Z., Métivier, L., & Collilieux, X. (2012). ITRF2008 plate motion model. *Journal of Geophysical Research*: *Solid Earth*, *117*(B7), Article B07402. https://doi.org/10.1029/2011JB008930

Altamimi, Z., Métivier, L., Rebischung, P., Collilieux, X., Chanard, K., & Barnéoud, J. (2023). ITRF2020 plate motion model. *Geophysical Research Letters*, *50*(24), Article e2023GL106373. https://doi.org/10.1029/2023GL106373

Argus, D. F., & Gordon, R. G. (1991). No-net-rotation model of current plate velocities incorporating plate motion model NUVEL-1. *Geophysical Research Letters*, *18*(11), 2039–2042. https://doi.org/10.1029/91GL01532

Argus, D. F., Gordon, R. G., & DeMets, C. (2011). Geologically current motion of 56 plates relative to the no-net-rotation reference frame. *Geochemistry*, *Geophysics*, *Geosystems*, *12*(11), Article Q11001. https://doi.org/10.1029/2011GC003751

Bird, P. (2003). An updated digital model of plate boundaries. *Geochemistry*, *Geophysics*, *Geosystems*, *4*(3), Article 1027. https://doi.org/10.1029/2001GC000252

Blewitt, G. (2008). Fixed point theorems of GPS carrier phase ambiguity resolution and their application to massive network processing: Ambizap. *Journal of Geophysical Research*: *Solid Earth*, *113*(B12), Article B12410. https://doi.org/10.1029/2008JB005736

Blewitt, G., & Lavallée, D. (2002). Effect of annual signals on geodetic velocity. *Journal of Geophysical Research*: *Solid Earth*, *107*(B7), ETG 9-1–ETG 9-11. https://doi.org/10.1029/2001JB000570

Bock, Y., Prawirodirdjo, L., Genrich, J. F., Stevens, C. W., McCaffrey, R., Subarya, C., Puntodewo, S. S. O., & Calais, E. (2003). Crustal motion in Indonesia from Global Positioning System measurements. *Journal of Geophysical Research*: *Solid Earth*, *108*(B8), Article 2367. https://doi.org/10.1029/2001JB000324

Boehm, J., Niell, A., Tregoning, P., & Schuh, H. (2006). Global Mapping Function (GMF): A new empirical mapping function based on numerical weather model data. *Geophysical Research Letters*, *33*(7), Article L07304. https://doi.org/10.1029/2005GL025546

Bos, M. S., & Scherneck, H. G. (2014). *Onsala Space Observatory*. http://holt.oso.chalmers.se/loading

DeMets, C., Gordon, R. G., & Argus, D. F. (2010). Geologically current plate motions. *Geophysical Journal International*, *181*(1), 1–80. https://doi.org/10.1111/j.1365-246X.2009.04491.x

Ghilani, C. D., & Wolf, P. R. (2006). *Adjustment computations*: *Spatial data analysis*. John Wiley & Sons. https://doi.org/10.1002/9780470121498

Goudarzi, M. A., Cocard, M., & Santerre, R. (2014). EPC: Matlab software to estimate Euler pole parameters. *GPS Solutions*, *18*(1), 153–162. https://doi.org/10.1007/s10291-013-0354-4

Kreemer, C., Blewitt, G., & Maerten, F. (2006). Co- and postseismic deformation of the 28 March 2005 Nias M_w 8.7 earthquake from continuous GPS data. *Geophysical Research Letters*, *33*(7), Article L07307. https://doi.org/10.1029/2005GL025566

Kreemer, C., Holt, W. E., & Haines, A. J. (2003). An integrated global model of present-day plate motions and plate boundary deformation. *Geophysical Journal International*, *154*(1), 8–34. https://doi.org/10.1046/j.1365-246X.2003.01917.x

Lyard, F., Lefevre, F., Letellier, T., & Francis, O. (2006). Modelling the global ocean tides: Modern insights from FES2004. *Ocean Dynamics*, *56*(5), 394–415. https://doi.org/10.1007/s10236-006-0086-x

McCaffrey, R. (2009). The tectonic framework of the Sumatran subduction zone. *Annual Review of Earth and Planetary Sciences*, *37*, 345–366. https://doi.org/10.1146/annurev.earth.031208.100212

Meade, B. J., & Hager, B. H. (2005). Block models of crustal motion in southern California constrained by GPS measurements. *Journal of Geophysical Research*: *Solid Earth*, *110*(3), 1–19. https://doi.org/10.1029/2004JB003209

Mustafar, M. A., Simons, W. J. F., Tongkul, F., Satirapod, C., Omar, K. M., & Visser, P. N. A. M. (2017). Quantifying deformation in North Borneo with GPS. *Journal of Geodesy*, *91*(10), 1241–1259. https://doi.org/10.1007/s00190-017-1024-z

Prawirodirdjo, L., & Bock, Y. (2004). Instantaneous global plate motion model from 12 years of continuous GPS observations. *Journal of Geophysical Research*: *Solid Earth*, *109*(B8), Article B08405. https://doi.org/10.1029/2003JB002944

Schmid, R., Rothacher, M., Thaller, D., & Steigenberger, P. (2005). Absolute phase center corrections of satellite and receiver antennas. *GPS Solutions*, *9*(4), 283–293. https://doi.org/10.1007/s10291-005-0134-x

Simons, W. J. F., Socquet, A., Vigny, C., Ambrosius, B. A. C., Haji Abu, S., Promthong, C., Subarya, C., Sarsito, D. A., Matheussen, S., Morgan, P., & Spakman, W. (2007). A decade of GPS in Southeast Asia: Resolving Sundaland motion and boundaries. *Journal of Geophysical Research*: *Solid Earth*, *112*(B6), Article B06420. https://doi.org/10.1029/2005JB003868

Vigny, C., Simons, W. J. F., Abu, S., Bamphenyu, R., Satirapod, C., Choosakul, N., Subarya, C., Socquet, A., Omar, K., Abidin, H. Z., & Ambrosius, B. A. C. (2005). Insight into the 2004 Sumatra-Andaman earthquake from GPS measurements in southeast Asia. *Nature*, *436*(7048), 201–206. https://doi.org/10.1038/nature03937

Yong, C. Z., Denys, P. H., & Pearson, C. F. (2017). Present-day kinematics of the Sundaland plate. *Journal of Applied Geodesy*, *11*(3), 169–177. https://doi.org/10.1515/jag-2016-0024

Zulkifli, N. A., Din, A. H. M., & Omar, A. H. (2019). The impact of different international terrestrial reference frames (ITRFs) on positioning and mapping in Malaysia. In *Lecture notes in civil engineering*: *Vol. 9. GCEC 2017* (pp. 671–690). Springer. https://doi.org/10.1007/978-981-10-8016-6_51

Zumberge, J. F., Heflin, M. B., Jefferson, D. C., Watkins, M. M., & Webb, F. H. (1997). Precise point positioning for the efficient and robust analysis of GPS data from large networks. *Journal of Geophysical Research*: *Solid Earth*, *102*(B3), 5005–5017. https://doi.org/10.1029/96JB03860